Weierstraß-Institut

für Angewandte Analysis und Stochastik

im Forschungsverbund Berlin e. V.

Preprint ISSN 0946 – 8633

Beyond the diffusion tensor model: The package dti

Jörg Polzehl[1], Karsten Tabelow[1]

submitted: November 9, 2010

[1] Weierstrass Institute
for Applied Analysis and Stochastics,
Mohrenstr. 39, 10117
Berlin, Germany
E-Mail: joerg.polzehl@wias-berlin.de
E-Mail: karsten.tabelow@wias-berlin.de

No. 1563

Berlin 2010

2010 *Mathematics Subject Classification.* 62P10, 92C55, 62H11, 62H35, 62G05 .

Key words and phrases. diffusion weighted imaging, high angular resolution, orientation distribution function, Q-ball imaging, angular central Gaussian distribution, tensor mixture model, order selection.

Edited by
Weierstraß-Institut für Angewandte Analysis und Stochastik (WIAS)
Mohrenstraße 39
10117 Berlin
Germany

Fax: +49 30 2044975
E-Mail: preprint@wias-berlin.de
World Wide Web: http://www.wias-berlin.de/

Abstract

Diffusion weighted imaging is a magnetic resonance based method to investigate tissue micro-structure especially in the human brain via water diffusion. Since the standard diffusion tensor model for the acquired data failes in large portion of the brain voxel more sophisticated models have bee developed.

Here, we report on the package **dti** and how some of these models can be used with the package.

1 Introduction

The basic principles of diffusion weighted imaging (DWI) have been introduced in the 1980's (Le Bihan and Breton, 1985; Merboldt *et al.*, 1985; Taylor and Bushell, 1985). Since then it has evolved into a beneficial technique for in-vivo investigation of tissue micro-structure in the human brain (Le Bihan *et al.*, 2001) and spinal cord (Clark *et al.*, 1999) as it probes microscopic structures well beyond typical image resolutions through water molecule displacement. Diffusion weighted data is measured using the pulsed gradient spin echo sequence (PGSE, Stejskal and Tanner, 1965) with a number of specified magnetic field gradients in different directions $\vec{q}$. Due to diffusion in tissue this signal $S(\vec{q})$ is attenuated compared to the signal S_0 acquired without gradient application. For a recent discussion of the physics of image acquisition, relations to white matter anatomy, clinical use and problems in neuroscience that can be addressed by DWI see e.g. Johansen-Berg and Behrens (2009).

In this paper we discuss the modeling and analysis of DWI data using the package **dti** (Tabelow and Polzehl, 2010, version 0.9-3) for the R environment for statistical computing (R Development Core Team, 2010). The first reference to this package that is restricted to diffusion tensor imaging (DTI) and adaptive smoothing within the context of the diffusion tensor model (Tabelow *et al.*, 2008) is Polzehl and Tabelow (2009) which refers to version 0.6-0.

The focus of this paper is on models for estimating the orientation density function (ODF), see Tuch *et al.* (2002); Wedeen *et al.* (2005); Aganj *et al.* (2010b) and Barnett (2009), that overcome the limitations of the tensor model. Such models are of special interest for high angular resolution diffusion weighted imaging (HARDI) data. Subsection 2.2 briefly reviews the diffusion tensor model and discusses its limitations. We then introduce both Q-ball imaging (see e.g. Tuch, 2004; Anderson, 2005; Hess *et al.*, 2006; Descoteaux *et al.*, 2007) and tensor mixture models (see e.g. Tabelow *et al.*, 2010, and references cited therein). Section 3 introduces the design of the package and illustrates its usage. Two appendices describe the data sets and code used for the examples. Data sets and scripts are provided in electronic form.

2 Modeling diffusion weighted data

2.1 The diffusion weighted signal

DWI effectively measures diffusion of water molecules, or more precisely protons within such a molecule in a direction determined by external magnetic field gradients. Let $P(\vec{r}, \vec{r}', \tau)$ denote the probability for a

Figure 1: Data visualization: $E(\vec{q},\tau)$ for a row of 4 voxel in data set 3

particle (spin) to diffuse from position $\vec{r}\,'$ to $\vec{r}$ in time τ. With DWI an aggregate value of P over a volume (voxel) V can be determined, i.e.

$$P(\vec{R},\tau) = \int_{\vec{r}\,'\in V,\ \vec{R}=\vec{r}-\vec{r}\,'} P(\vec{r},\vec{r}\,',\tau)p(\vec{r}\,')d\vec{r}\,', \tag{1}$$

where $p(\vec{r}\,')$ is the initial spin density. V is typically of a size of about $1\times1\times1$ mm^3. The relation to the normalized diffusion weighted signal $E(\vec{q},\tau) = S(\vec{q},\tau)/S_0$, is given by the three-dimensional Fourier transform $\mathcal{F}$:

$$\begin{aligned} P(\vec{R},\tau) &= \int_{\mathbb{R}^3} E(\vec{q},\tau)\, e^{-2\pi i\vec{q}\,\vec{R}} d\vec{q} = \mathcal{F}(E(\vec{q},\tau)),\\ E(\vec{q},\tau) &= \int_{\mathbb{R}^3} P(\vec{R},\tau)\, e^{2\pi i\vec{q}\,\vec{R}} d\vec{R} = \mathcal{F}^{-1}(P(\vec{q},\tau)). \end{aligned} \tag{2}$$

2.2 The diffusion tensor model

Assuming homogeneity within a voxel the diffusion tensor model is derived for the special case of free anisotropic Gaussian diffusion[1], i.e.

$$P(\vec{R},\tau) = P(r\vec{u},\tau) = \frac{1}{\sqrt{\det \mathcal{D}(4\pi\tau)^3}} \exp\left(-r^2\frac{\vec{u}^T\mathcal{D}^{-1}\vec{u}}{4\tau}\right).$$

The relation (2) can then be expressed as

$$E(\vec{q},\tau) = E(q\vec{u},\tau) = e^{-b\vec{u}^T\mathcal{D}\vec{u}}$$

with the b-value depending on q and the effective diffusion time τ (Basser *et al.*, 1994a). Within this model diffusion is completely characterized by the positive definite symmetric 3×3 matrix $\mathcal{D}$, the diffusion tensor.

The components of the diffusion tensor clearly depend on the orientation of the object in the scanner frame. Only rotationally invariant quantities derived from the diffusion tensor circumvent this dependence

[1] Note, that the Gaussian model of diffusion can be considered as the low spatial frequency approximation to the diffusion propagator (Tuch *et al.*, 2002) in case of restricted diffusion.

and are usually used for further analysis, mainly based on the eigenvalues μ_i $(i = 1, 2, 3)$ of $\mathcal{D}$ with $\mu_i > 0$ for positive definite tensors. The eigenvector $\vec{e}_1$ corresponding to the principal eigenvalue μ_1 determines the main diffusion direction used for fiber tracking.

The simplest quantity based on the eigenvalues is the trace of the diffusion tensor $Tr(\mathcal{D}) = \sum_{i=1}^{3} \mu_i$ which is related to the mean diffusivity $\langle\mu\rangle = Tr(D)/3$. The anisotropy of the diffusion can be described using higher moments of the eigenvalues μ_i. The widely used fractional anisotropy (FA) is defined as

$$FA = \sqrt{\frac{3}{2}} \sqrt{\sum_{i=1}^{3} (\mu_i - \langle\mu\rangle)^2 \; / \; \sum_{i=1}^{3} \mu_i^2}$$

with $0 \leq FA \leq 1$, where $FA = 0$ indicates equal eigenvalues and hence no diffusion anisotropy.

The resulting FA-maps together with a color-coding scheme are helpful for medical diagnostics. The principal eigenvector $\vec{e}_1 = (e_{1x}, e_{1y}, e_{1z})$ is used for assigning each voxel a specific color, interpreting e_{1x}, e_{1y}, and e_{1z} weighted with the value FA as red, green, and blue contribution

$$(R, G, B) = (|e_{1x}|, |e_{1y}|, |e_{1z}|) \cdot FA. \tag{3}$$

Note, that in contrast to the eigenvalues and the fractional anisotropy the principal eigenvector and hence the color coding depend on the orientation of the object in the scanner frame.

The main problem of diffusion tensor imaging arises from the assumption of homogeneity within a voxel. Diffusion weighted imaging aims to detect structures with an extension of up to $15cm$ and a diameter of about $30\mu m$. A high percentage of voxel contains structures with different orientation. In such a situation partial volume effects may lead to non informative tensor estimates.

2.3 The orientation density function

The drawbacks of the diffusion tensor model can be avoided by a more detailed analysis of Eq. (1). The main interest in diffusion weighted imaging is to access the orientation properties of the tissue, i.e. in case of brain imaging of neuronal fiber bundles. This means that our main interest is in the orientation properties of the probability distribution P, i.e. its projection onto the unit sphere

$$\mathrm{ODF}(\vec{u}) = \int_0^\infty r^2 P(r\vec{u}) dr, \tag{4}$$

with $\vec{R} = r\vec{u}$ and $\vec{u} \in S^2$ and neglecting the dependence on τ. Eq. (4) is the orientation distribution function as proposed in Wedeen *et al.* (2005) and used in Aganj *et al.* (2010b). For a detailed discussion on how this differs from the original definition of Tuch *et al.* (2002) see Barnett (2009).

This definition is intrinsically normalized

$$\int_{S^2} \mathrm{ODF}(\vec{u}) d\vec{u} = 1$$

and defines a probability distribution on the sphere S^2.

In case of elliptically symmetric distributions $P(\vec{R}, \tau) = C_\tau (\det \mathcal{D})^{-1/2} h_\tau \left(\vec{R}^\top \mathcal{D}^{-1} \vec{R} \right)$ with zero mean, shape parameter $\mathcal{D}$, some function h_τ and normalization constant C_τ the ODF is given by

$$\mathrm{ODF}(\vec{u}) = \frac{1}{4\pi\sqrt{\det \mathcal{D}}} \sqrt{\frac{1}{(\vec{u}^T \mathcal{D}^{-1} \vec{u})^3}},$$

(see Tabelow *et al.*, 2010). This is known as the *angular central Gaussian distribution* (Mardia and Jupp, 2000) on the sphere. One example for an elliptically symmetric distribution P is the anisotropic Gaussian diffusion assumed for the tensor model.

Using spherical coordinates $\vec{q} = (q, \theta, \phi)$ the orientation distribution function can be expressed as a function of the signal $E(\vec{q})$:

$$\mathrm{ODF}(\vec{u}) = \frac{1}{4\pi} - \frac{1}{8\pi^2} \int_0^{2\pi} \int_0^{\infty} \frac{1}{q} \nabla_b^2 E(\vec{q}) dq d\phi$$
$$\nabla_b^2 E = \frac{1}{\sin\theta} \frac{\delta}{\delta\theta} (\sin\theta \frac{\delta E}{\delta\theta}) + \frac{1}{\sin^2\theta} \frac{\delta E}{\delta\phi^2}$$

where ∇_b^2 is the Laplace-Beltrami operator, see e.g. Aganj *et al.* (2010b).

2.4 Q-Ball imaging

Q-ball imaging (QBI) (Tuch, 2004) aims at the reconstruction of the orientation distribution function from signals $E(\vec{q_0})$ measured on one q-shell, i.e. for one fixed b-value. This is in contrast to alternative methods like diffusion spectrum imaging (DSI) (Wedeen *et al.*, 2005) or hybrid diffusion imaging (HYDI) (Wu and Alexander, 2007) which measure diffusion weighted images on a Cartesian grid of diffusion gradients or sample gradients from spheres with different b-values, effectively requiring significantly more diffusion weighted images.

QBI requires an extrapolation of the signal $E(\vec{q_0})$ to other locations in q-space in order to evaluate the integral over q. Here, we use the formulation of QBI as in Aganj *et al.* (2010b) which differs from the original proposal by Tuch (2004) by the r^2 weighting factor in the definition of the ODF. The extrapolation of $E(\vec{q_0})$ can be done by assuming a mono-exponential decay of the signal in q

$$E(q\vec{u}) = E(q_0\vec{u})^{\frac{q^2}{q_0^2}}$$

Under this assumption the ODF can be expressed as

$$\mathrm{ODF}(\vec{u}) = \frac{1}{4\pi} - \frac{1}{16\pi^2} \mathrm{FRT}\{\nabla_b^2 \ln(-\ln E(\vec{u}))\}$$

where

$$\mathrm{FRT}(f(\vec{u})) = \iint_{\vec{u}^\perp} f(\vec{w}) \delta(|\vec{w}| - 1) d\vec{w}$$

denotes the Funk-Radon transformation, see again Aganj *et al.* (2010b) for details.

Efficient implementations of QBI make use of the spherical harmonics basis functions Y_k^m, particularly in form of the real symmetric modified basis. For selected maximum order l, even order $k \leq l$, and $-k \leq m \leq k$ we define an index $j = k(k+1)/2 + m + 1$ and a real function

$$Y_j = \begin{cases} \sqrt{2}\Re(Y_k^m) & -k \leq m < 0 \\ Y_k^0 & m = 0 \\ \sqrt{2}\Im(Y_k^m) & 0 < m \leq k \end{cases}$$

using the real part $\Re(Y_k^m)$ and the imaginary part $\Im(Y_k^m)$ of Y_k^m, see Descoteaux *et al.* (2007). The spherical harmonics Y_j are eigenfunctions of the Laplace-Beltrami operator, i.e. that $\nabla_b^2 Y_j(\vec{u}) =$

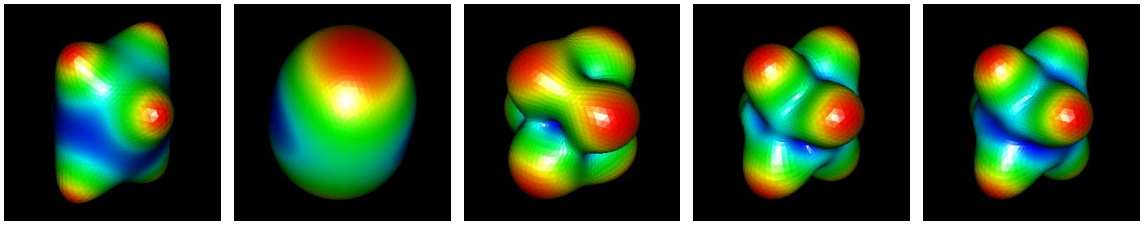

Figure 2: True ODF and expected reconstruction by spherical harmonics expansion of order 2, 4, 6 and 8 (from left to right)

$-k_j(k_j+1)Y_j(\vec{u})$, where k_j is the order associated with j. The use of the expansion

$$\ln(-\ln(E(\vec{u}))) \approx \sum_{j=1}^{N} c_j Y_j, \qquad N = (l+1)(l+2)/2 \tag{5}$$

leads to an approximation of the ODF by

$$\mathrm{ODF}(\vec{u}) \approx \frac{1}{4\pi} + \frac{1}{8\pi} \sum_{j=1}^{N} c_j k_j (k_j+1) P_{k_j}(0) Y_j \tag{6}$$

where $P_{k_j}()$ are the Legendre polynomials of order k_j, see again Aganj *et al.* (2010b). Estimation of the ODF is now a linear problem where estimates of the parameters are obtained by solving a regularized least squares problem, see Descoteaux *et al.* (2007); Aganj *et al.* (2010b). Figure 2 illustrates effects of Q-ball reconstruction by spherical harmonics expansion for a voxel where the true ODF is a mixture of three angular central Gaussian distributions. Reconstruction was based on 136 gradient directions in a noise-free situation. See Appendix B for the R-code used to generate the Figure.

2.5 Tensor mixture models

Although the estimation of the ODF by spherical harmonics expansion of the observed signal is computationally appealing it also has several drawbacks. The form of the ODF reconstruction depends on the order l of the approximation and the amount of regularization used. The location of maxima is usually biased. Finally, in the case of QBI, the result heavily depends on the assumption of a mono-exponential decay of the signal E with q.

Lets assume a voxel to contain M compartments covering a fraction w_m of the voxel ($\sum_{m=1}^{M} w_m = 1$) and free anisotropic Gaussian diffusion characterized by the tensor $\mathcal{D}_m$ in compartment m, $m = 1, \ldots, M$. This leads to a signal that does not exhibit a mono-exponential decay but is

$$E(\vec{q}) = \sum_{m=1}^{M} w_m \exp(-b\vec{u}^T \mathcal{D}_m \vec{u}). \tag{7}$$

The corresponding ODF is a mixture of of the ODF's for the compartments

$$\mathrm{ODF}(\vec{u}) = \sum_{m=1}^{M} w_i \frac{1}{4\pi\sqrt{\det \mathcal{D}_m}} \sqrt{\frac{1}{(\vec{u}^T \mathcal{D}_m^{-1} \vec{u})^3}}.$$

This additivity of the ODF is not preserved when using Eqs. (5,6) due to the non-linearity of $\ln(-\ln(\cdot))$.

The mixture model of M diffusion tensors $\mathcal{D}_i$ in its general form (7) (see e.g. Tuch, 2002; Alexander, 2005, 2006; Özarslan *et al.*, 2006), is too flexible, leading to severe identifiability and numerical problems (Tuch, 2002; Johansen-Berg and Behrens, 2009). Suggestions to resolve the problem include the restriction of the number of components M to 2 (Alexander, 2005, 2006; Özarslan *et al.*, 2006), the approximation of the solution by estimating the ODF spherical harmonics expansion and subsequent deconvolution (Tournier *et al.*, 2004) or the use of restrictions for the tensor eigenvalues (Leow *et al.*, 2009).

In (Tabelow *et al.*, 2010) we show that a reduction of the complexity of the model accompanied by model selection using BIC (Schwarz, 1978) is practicable. We assume the diffusion tensors $\mathcal{D}_m$ to have a spectral decomposition $\mathcal{D}_m = \lambda_1 d_m d_m^T + \lambda_2(I_3 - d_m d_m^T)$, i.e. to be prolate ($\lambda_1 > \lambda_2 = \lambda_3$, Basser *et al.*, 1994b) and to differ only in their main direction d_m. After reparametrization the reduced model has the form

$$E(\vec{q}) = \sum_{m=1}^{M} \tilde{w}_m \exp(-b\vartheta(\vec{q}^{\top} d_m)^2), \quad \tilde{w}_m \geq 0, \quad \sum_{m=1}^{M} \tilde{w}_m < 1, \quad \vartheta \geq 0$$

with $\lambda_2 = -\frac{1}{b} log \sum_{m=1}^{M} \tilde{w}_m$, $\lambda_1 = \vartheta + \lambda_2$ and $w_m = \tilde{w}_m / \sum_{l=1}^{M} \tilde{w}_l$.

With $d_m = (\sin(\phi_m)\cos(\eta_m), \sin(\phi_m)\sin(\eta_m), \cos(\phi_m))$ the model has $2M + 1$ nonlinear parameters and M linear parameters with constraints. For a detailed description of parameter estimation and a strategy to select the number of mixture components M we refer to (Tabelow *et al.*, 2010). The tensor mixture model is characterized by the selected order p_{opt}, the fractional anisotropy

$$FA = \frac{(\lambda_1 - \lambda_2)}{\sqrt{\lambda_1^2 + 2 \cdot \lambda_2^2}},$$

and the effective order

$$EO = \sum_{m=1}^{p_{opt}} (2m - 1) w_m \ .$$

2.6 Fiber tracking

The estimated diffusion tensors and ODF's can be used to infer on the underlying neuronal fiber structure. Usually this is performed using fiber tracking algorithms on vector fields or tensor orientation functions extracted from the estimated objects. There exists a large variety of fiber tracking algorithms that can be roughly classified into deterministic and probabilistic approaches and are based either on local or global criteria. For an overview on existing approaches see e.g. (Mori and van Zijl, 2002; Behrens *et al.*, 2007; Descoteaux *et al.*, 2009; Reisert *et al.*, 2010; Wu *et al.*, 2009; Zhang *et al.*, 2009; Aganj *et al.*, 2010a). For this paper we use the FACT algorithm proposed in Xue *et al.* (1999); Mori *et al.* (1999). This is also implemented within **dti**.

3 Analyzing DWI data: The R-package dti

The package **dti** for the R statistical environment (R Development Core Team, 2010) has been designed to perform an analysis of diffusion weighted imaging data. The implementation uses S4-classes. For detailed information we refer to the documentation of the package. Information on the package and its classes and methods can be obtained within an R-session by

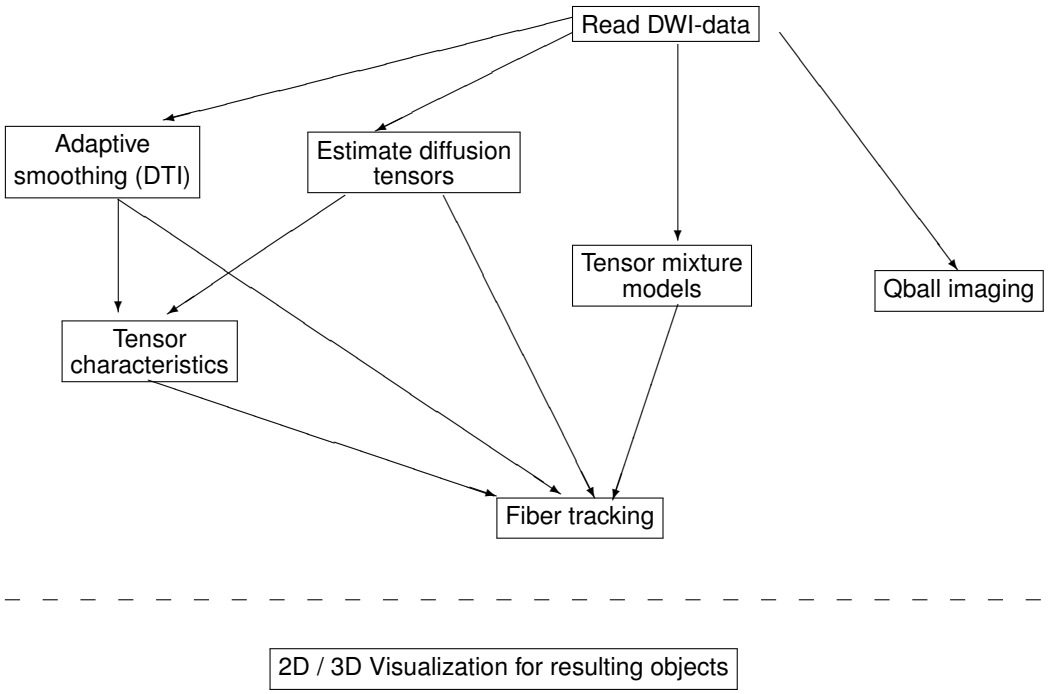

Figure 3: Work flow for analyzing DWI data with package **dti**

```
> library(dti)
> help(dti)
> class?class-name
> methods?method-name
```

Figure 3 illustrates the anticipated work flow for analyzing DWI data. Tables 1, 2 and 3 provide an overview on currently implemented classes, functions and methods.

Table 1: Overview on package **dti**: classes

Class	Content	Ref.
`dwi`	Basic class containing data description	(1)
`dtiData`	DWI data objects. Extends (1).	(2)
`dtiTensor`	Estimated diffusion tensor. Extends (1).	(3)
`dtiIndices`	Estimated diffusion tensor indices and orientations. Extends (1).	(4)
`dwiMixtensor`	Estimated tensor mixtures. Extends (1).	(5)
`dwiQball`	Estimated Q-ball using spherical harmonics. Extends (1).	(6)
`dwiFiber`	Fiber tracking results. Extends (1).	(7)

The package includes two data sets, `"polyeder"`, containing a description of regular polyeders that are refinements of the icosahedron and are used for visualization and a dataset containing sets of optimal gradient directions `"optgradients"`.

Currently there are two comprehensive demos, `demo(dti_art)` for modeling within the context of the diffusion tensor model (DTI) and `demo(mixtens_art)` illustrating the work flow for analyzing

Table 2: Overview on package **dti**: functions

Function	Purpose	creates
`dtiData`	Create DWI data object from binary image file	(1)
`readDWIdata`	Read DWI-Data using capabilities of package **fmri**	(1)
`tensor2medinria`	Write tensor estimates as NIfTI	
`medinria2tensor`	Read tensor estimates from NIfTI.	(3)

Table 3: Overview on package **dti**: methods

Method	Purpose	defined for classes	creates
`dtiTensor`	Compute diffusion tensor estimates	(2)	(3)
`dti.smooth`	Adaptive smoothing for DTI	(2)	(3)
`dtiIndices`	Compute diffusion tensor characteristics	(3)	(4)
`dwiQball`	Q-ball imaging using spherical harmonics	(2)	(6)
`dwiMixtensor`	estimate tensor mixtures	(2)	(5)
`tracking`	streamline fiber tracking	(3,4,5)	(7)
`selectFibers`	select subset of fiber tracks	(7)	(7)
`reduceFibers`	remove redundant fiber tracks	(7)	(7)
`extract`	extract information or components	(2,3,4,5,6)	
`"["`	index operations	(2,3,4,5,6)	(2,3,4,5,6)
`summary`	summarize information	(2,3,4,5,6,7)	
`plot`	plot-method	(2,3,4,5,7)	
`show`	object descriptions	(2,3,4,5,6,7)	
`print`	object descriptions	(2,3,4,5,6,7)	
`show3d`	3D visualization of objects	(2,3,4,5,6,7)	

HARDI data. In both demos a variety of configurations can be specified both concerning underlying true fiber structures as well as number of gradients and SNR.

3.1 Examples

We illustrate the capabilities of the package using a series of examples. For the code we refer to Appendix B.

3.1.1 Example 1: Tensor estimates

This example uses the data set 3 from Appendix A to illustrate the capabilities of the package in diffusion tensor imaging in an adequate situation. See corresponding code in Appendix B. Voxel wise tensor estimates are obtained without and with structural adaptive smoothing (maximal bandwidth 4), tensor characteristics are computed and fiber tracking is performed. Figure 4 provides a 2D projection of a 3D visualization of tensor characteristics and fiber tracking results. Orientations are color coded using Eq. (3). Note the improvement of results due to adaptive smoothing. For details we refer to (Tabelow *et al.*, 2008; Polzehl and Tabelow, 2009)

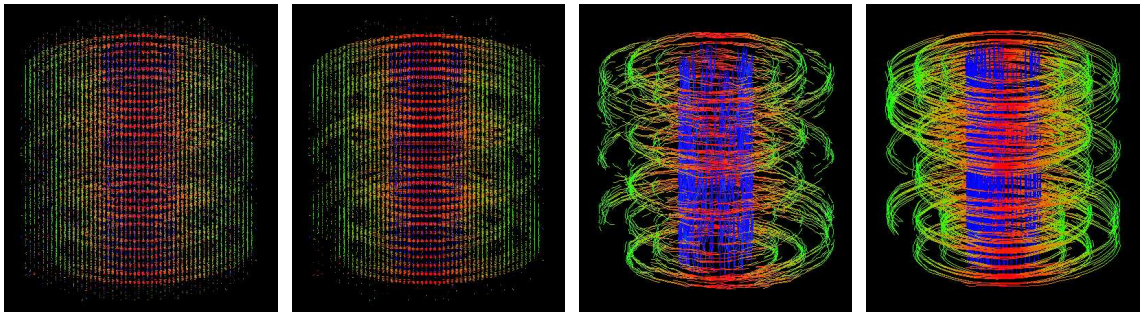

Figure 4: 3D visualization of main tensor orientations without and with use of spatially adaptive smoothing and corresponding fiber tracking results (from left to right). Shown are results for voxel with estimated $FA > 0.3$ and fiber tracks starting from such voxel. You may run the example code to see more projections.

3.1.2 Example 2: The effect of regularization in Q-ball imaging

The next example illustrates the effect of regularization in Q-ball reconstruction with spherical harmonics. We use data set 1 from Appendix A. The data are modeled using a tensor mixture model of maximum order 4 and the ODF-estimate (5, 6) applying the regularization proposed in (Aganj *et al.*, 2010b) when estimating the coefficients in (5). The regularization parameter is chosen as $\lambda = 2.5 * 10^{-3}, 1 * 10^{-2}$ and $4 * 10^{-2}$, respectively. Coordinates of two voxel with structure have been determined interactively using

```
coord <- plot(mixtensobj, slice = 3, what = "eorder",
              view = "axial", identify = TRUE)
```

These voxel have been used in the two rows of Figure 5. Especially in the first row it is difficult to interpret the results from Q-ball reconstruction using Eqs. (5,6). Note the strong impact of the regularization parameter on the results.

3.1.3 Example 3: Tensor mixture models

Here we illustrate some capabilities of the tensor mixture model in comparison to the tensor model. We first analyze the data in data set 2 from Appendix A with both models. Figure 6 provides characteristics of results obtained in the analysis. The left image shows a color coded FA for the second axial slice obtained using the tensor model. The other four images provide FA, estimated number of mixture components, effective order and maximal eigenvalues (from left to right) for the same slice obtained employing a tensor mixture model with specified maximal number of compartments of 5 (see Tabelow *et al.*, 2010, for definitions and more explanation). We observe an increase of FA in comparison with the tensor model, especially in regions adjacent to tissue borders (Tabelow *et al.*, 2010). Note the spatial homogeneity observed in all characteristics for the tensor mixture model. Figure 7 illustrated some capabilities in 3D visualization. The image shows estimated ODF's for all voxel with effective order larger or equal than 1.8 together with fiber tracks starting from these voxel.

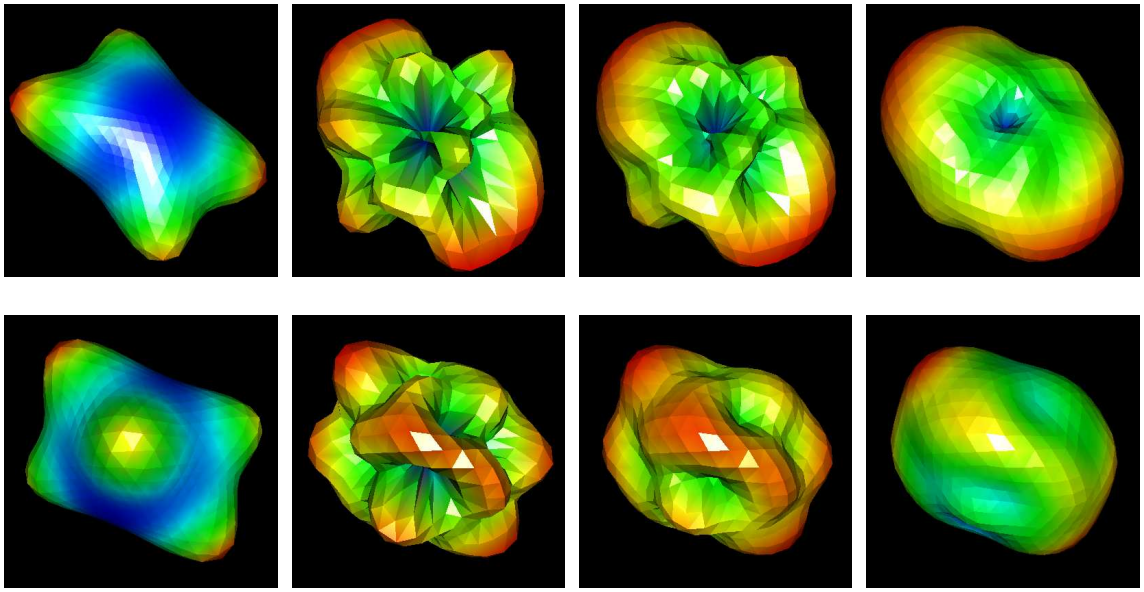

Figure 5: ODF estimated using tensor mixture models (left) and using Q-Ball reconstruction with spherical harmonics of order 8 and regularization parameter $\lambda = 2.5 * 10^{-3}, 1 * 10^{-2}, 4 * 10^{-2}$ (from left to right) for two interactively selected voxel. You may run the example code to see more projections.

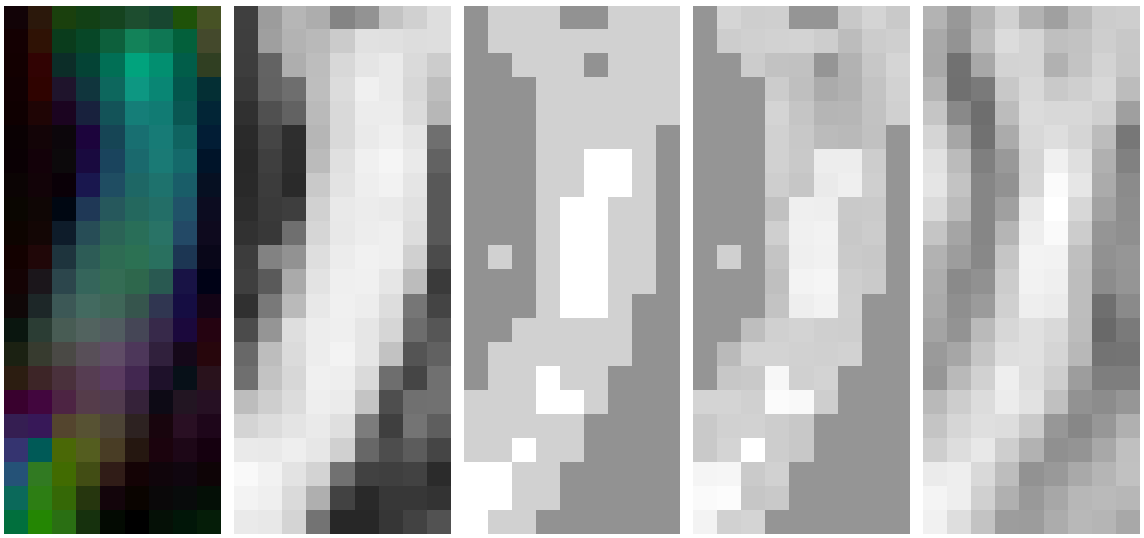

Figure 6: visualization of results for data set 2, axial slice 2: Color coded FA (tensor model), FA, number of mixture components, effective order and maximal eigenvalue for mixture model with maximum model order 5 (from left to right).

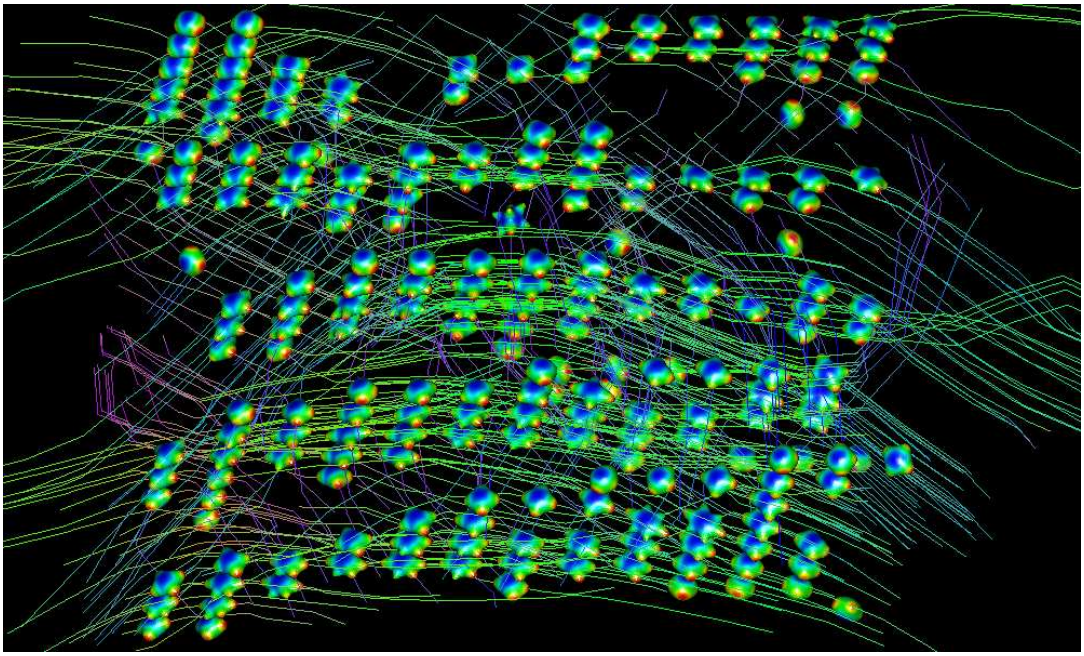

Figure 7: 3D visualization of results for data set 2: Voxel with estimated effective order larger than 1.8 and fibertracks starting within these voxel. You may run the example code to see more projections.

3.1.4 Example 4: Fiber tracking

The object `tracks100` provided as data set 5 has been obtained analyzing high resolution DWI data recorded by H.-U. Voss at Weill Medical College, Cornell University NY. 140 gradient directions were used and images of $256 \times 256 \times 66$ voxel with spatial resolution of approximately $.9mm \times .9mm \times 1.8mm$ where recorded. A history of the object `tracks100` and its basic characteristics can be obtained by

```
> summary(tracks100)

  Object of class dwiFiber
  Generated by calls    :
[[1]]
readDWIdata(gradient, "s0004", "DICOM", 66, level = 0.75)

[[2]]
dwiMixtensor(data, maxcomp = 5, reltol = 1e-07, nguess = 5000)

[[3]]
tracking(nymix5, minfa = 0.266)

[[4]]
selectFibers(nymix5tracks1, minlength = 100)

  Source-Filename       : s0004
  Dimension             : 256x256x66
  Number of Gradients   : 150
```

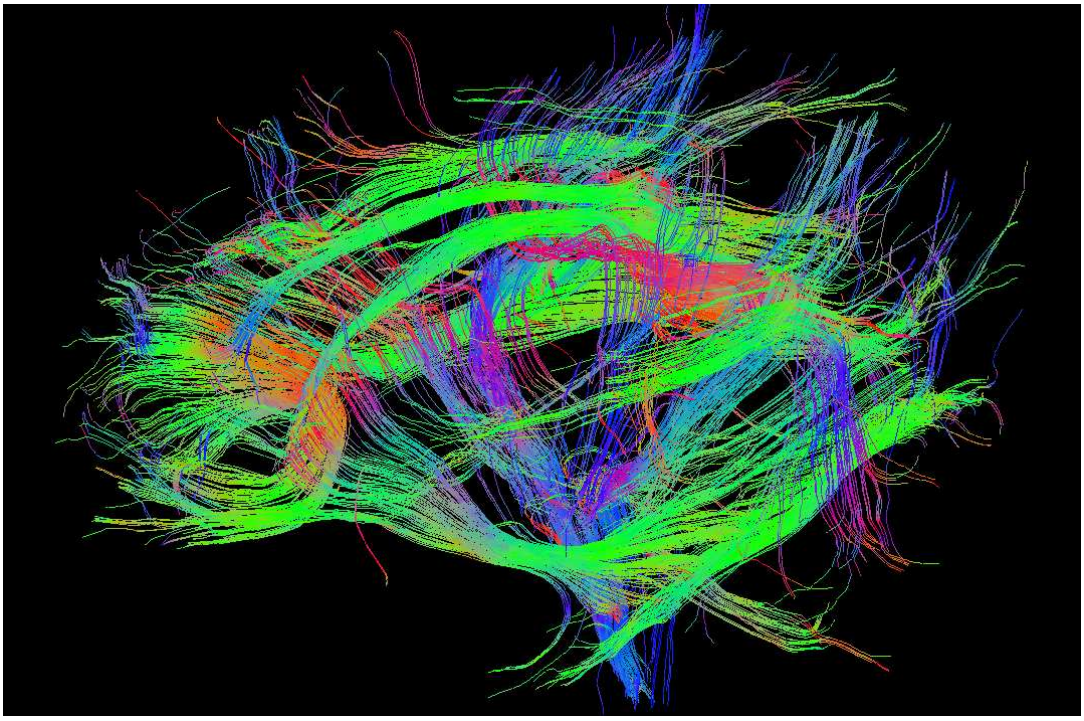

Figure 8: Visualization of fiber tracks with minimal length 100.

```
  Voxel extensions      : 0.8984x0.8984x1.8
  Minimum FA  : 0.266
  Maximum angle : 30
  Number of fibers : 1904
  Quantiles of fiber lengths:
    0%    25%    50%    75%   100%
100.00 107.00 117.00 136.25 256.00
  Total number of line segments : 237612
```

Figure 8 provides an illustration of the main long fiber tracks revealed by the analysis.

Acknowledgments

This work is supported by the DFG Research Center MATHEON. We thank H.-U. Voss for agreeing to make the experimental data used in this paper publicly available under GPL ≥ 2

References

Aganj I, Lenglet C, Jahanshad N, Yacoub E, Harel N, Thompson P, Sapiro G (2010a). "A Hough transform global probabilistic approach to multiple-subject diffusion MRI tractography." *Technical Report 2305*, University of Minnesota, IMA.

Aganj I, Lenglet C, Sapiro G, Yacoub E, Ugurbil K, Harel N (2010b). "Reconstruction of the Orienta-

tion Distribution Function in Single- and Multiple-Shell q-Ball Imaging Within Constant Solid Angle." *Magnetic Resonance in Medicine*, **64**, 554–556.

Alexander DC (2005). "Multiple-Fiber Reconstruction Algorithms for Diffusion MRI." *Annals of the New York Acadamy of Sciences*, **1064**, 113–133.

Alexander DC (2006). "An Introduction to computational diffusion MRI: the diffusion tensor and beyond." In J Weickert, H Hagen (eds.), *Visualization and image processing of tensor fields*. Springer.

Anderson A (2005). "Measurements of fiber orientation distributions using high angular resolution diffusion imaging." *Magnetic Resonance in Medicine*, **54**, 1194–1206.

Barnett A (2009). "Theory of Q-ball Imaging Redux: Implications for Fibre Tracking." *Magnetic Resonance in Medicine*, **62**, 910–923.

Basser P, Mattiello J, Le Bihan D (1994a). "Estimation of the effective self-diffusion tensor from the NMR spin echo." *Journal of Magnetic Resonance B*, **103**, 247–254.

Basser PJ, Mattiello J, Le Bihan D (1994b). "MR Diffusion Tensor Spectroscopy and Imaging." *Biophysical Journal*, **66**, 259–267.

Behrens TEJ, Johansen-Berg H, Jbabdi S, Rushworth MFS, Woolrich MW (2007). "Probabilistic diffusion tractography with multiple fibre orientations: What can we gain?" *Neuroimage*, **34**, 144–155.

Clark CA, Barker GJ, Tofts PS (1999). "Magnetic Resonance Diffusion Imaging of the Human Cervical Spinal Cord in Vivo." *Magnetic Resonance in Medicine*, **41**, 1269–1273.

Descoteaux M, Angelino E, Fitzgibbons S, Deriche R (2007). "Regularized, Fast and Robust Analytical Q-Ball Imaging." *Magnetic Resonance in Medicine*, **58**, 497–510.

Descoteaux M, Deriche R, Knösche TR, Anwander A (2009). "Deterministic and Probabilistic Tractography based on Complex Fiber Orientation Distributions." *IEEE Transactions on Medical Imaging*, **28**, 269–286.

Hess C, Mukherjee P, Han E, Xu D, Vigneron D (2006). "Q-ball reconstruction of multimodal fiber orientations using the spherical harmonic basis." *Magnetic Resonance in Medicine*, **56**, 104–117.

Johansen-Berg H, Behrens TEJ (2009). *Diffusion MRI: From Quantitative Measurement to In-Vivo Neuroanatomy*. Academic Press.

Le Bihan D, Breton E (1985). "Imagerie de Diffusion in Vivo par Résonance Magnétique Nucléaire (Invivo Magnetic Resonance Imaging of Diffusion)." *Comptes rendus de l'Académie des Sciences. La vie des sciences*, **301**, 1109–1112.

Le Bihan D, Mangin JF, Poupon C, Clark CA, Pappata S, Molko N, Chabriat H (2001). "Diffusion Tensor Imaging: Concepts and Applications." *Journal of Magnetic Resonance*, **13**, 534–546.

Leow A, Zhu S, McMahon K, de Zubicaray G, Meredith M, Wright M, Thompson P (2009). "The tensor distribution function." *Magnetic Resonance in Medicine*, **61**, 205–214. University of California, Los Angeles, CA, USA.

Mardia KV, Jupp PE (2000). *Directional Statistics*. Wiley.

Merboldt KD, Hanicke W, Frahm J (1985). "Self-Diffusion NMR Imaging Using Stimulated Echoes." *Journal of Magnetic Resonance*, **64**, 479–486.

Mori S, Crain BJ, Chacko VP, van Zijl PCM (1999). "Three dimensional tracking of axonal projections in the brain by magnetic resonance imaging." *Annals of Neurology*, **45**, 265–269.

Mori S, van Zijl PCM (2002). "Fibre tracking: principles and strategies - a technical review." *NMR in Biomedicine*, **15**, 468–480.

Özarslan E, Shepherd TM, Vemuri BC, Blackband SJ, Mareci TH (2006). "Resolution of complex tissue microarchitecture using the diffusion orientation transform (DOT)." *Neuroimage*, **31**, 1086–1103.

Polzehl J, Tabelow K (2009). "Structural Adaptive Smoothing in Diffusion Tensor Imaging: The R Package dti." *Journal of Statistical Software*, **31**(9), 1–23.

R Development Core Team (2010). *R: A Language and Environment for Statistical Computing*. R Foundation for Statistical Computing, Vienna, Austria. ISBN 3-900051-07-0, URL `http://www.R-project.org`.

Reisert M, Mader I, Anastasopoulos C, Weigel M, Schnell S, Kiselev V (2010). "Global fiber reconstruction becomes practical." *Neuroimage*. doi:10.1016/j.neuroimage.2010.09.016.

Schwarz G (1978). "Estimating the dimension of a model." *Annals of Statistics*, **6**, 461–464.

Stejskal EO, Tanner JE (1965). "Spin diffusion measurements: spin echoes in the presence of a time-dependent field gradient." *The Journal of Chemical Physics*, **42**, 288–292.

Tabelow K, Polzehl J (2010). *dti: DTI/DWI Analysis*. R package version 0.9-3, URL `http://CRAN.R-project.org/package=dti`.

Tabelow K, Polzehl J, Spokoiny V, Voss HU (2008). "Diffusion Tensor Imaging: Structural adaptive smoothing." *Neuroimage*, **39**, 1763–1773.

Tabelow K, Voss HU, Polzehl J (2010). "Modeling the orientation distribution function by mixtures of angular central Gaussian distributions." *Technical Report 1559*, WIAS, Berlin.

Taylor DG, Bushell MC (1985). "The Spatial Mapping of Translational Diffusion Coefficients by the NMR Imaging Technique." *Physics in Medicine and Biology*, **30**, 345–349.

Tournier JD, Calamante F, Gadian DG, Connelly A (2004). "Direct estimation of the fiber orientation density function from diffusion-weighted MRI data using spherical deconvolution." *Neuroimage*, **23**, 1176–1185.

Tuch DS (2002). *Diffusion MRI of Complex Tissue Structure*. Ph.D. thesis, Massachusetts Institute of Technology.

Tuch DS (2004). "Q-Ball Imaging." *Magnetic Resonance in Medicine*, **52**, 1358–1372.

Tuch DS, Reese TG, Wiegell MR, Makris N, Belliveau JW, Wedeen VJ (2002). "High angular resolution diffusion imaging reveals intravoxel white matter fiber heterogeneity." *Magnetic Resonance in Medicine*, **48**, 577–582.

Wedeen VJ, Hagmann P, Tseng WY, Reese TG, Weisskopf RM (2005). "Mapping complex tissue architecture with diffusion spectrum imaging." *Magnetic Resonance in Medicine*, **54**, 1377–1386.

Wu X, Xu Q, Xu L, Zhou J, Anderson AW, Ding Z (2009). "Genetic white matter fiber tractography with global optimization." *Journal of Neuroscience Methods*, **184**, 375–379.

Wu YC, Alexander A (2007). "Hybrid diffusion imaging." *Neuroimage*, **36**, 617–629.

Xue R, van Zijl PCM, Crain BJ, Solaiyappan M, Mori S (1999). "In vivo three-dimensional reconstruction of rat brain axonal projections by diffusion tensor imaging." *Magnetic Resonance in Medicine*, **42**, 1123–1127.

Zhang F, Hancock ER, Goodlett C, Gerig G (2009). "Probabilistic white matter fiber tracking using particle filtering and von Mises-Fisher sampling." *Medical Image Analysis*, **13**, 5–18.

A Data sets

With this document we provide four data sets that have been used within the text and can be used to explore the capabilities of the R package **dti**. The data are contained in the electronic appendix of this paper in form of directories containing NIfTI-Files. The data may be freely used under the terms of the GPL ≥ 2 license.

MRI images were obtained from a healthy male volunteer in the age group 40 - 45 within an Institutional Review Board approved research protocol at Weill Cornell Medical College. Images were acquired on a 3.0 Tesla General Electric Excite MRI scanner using an 8-channel receive-only head coil. First, a localizer scan was obtained to prescribe the position of the subsequent DWI scan. For the DWI scan, a single-shot spin-echo EPI sequence with 10 images without diffusion weighting and 140 diffusion gradient directions, which were approximately isotropically distributed over the sphere, was used, with an echo and repetition time of TE = 73.2 ms and TR = 14000 ms, respectively. 66 axial slices were scanned with no skip and an acquisition matrix size of 128 $\times$ 128. Images were zero-filled to an image matrix size of 256 $\times$ 256, yielding an effective resolution of 0.898 $\times$ 0.898 $\times$ 1.800 mm^3. The b-value in the diffusion weighted images was 1000 s/mm^2, the parallel imaging acceleration factor was 2, and the total scan time for this scan was 36 min.

Data set 1: This data set contains a sub cube of the DWI data described above. The data covers parts of the Genu of the Corpus Callosum (GCC), the Anterior Talamic Radiation (ATR) and the Superior Fronto-Occipital-Fasciculus (SFO).

Data directory: data1

Dimension: $40 \times 40 \times 5$

Gradient-File: b-directions.txt

Number of gradients: 150 (10 zero, 140 directions)

Data set 2: This data set contains a sub cube of the DWI data described above. The sub cube contains a contiguous region where three main directions of diffusion are found.

Data directory: data2

Dimension: $9 \times 22 \times 5$

Gradient-File: b-directions.txt

Number of gradients: 150 (10 zero, 140 directions)

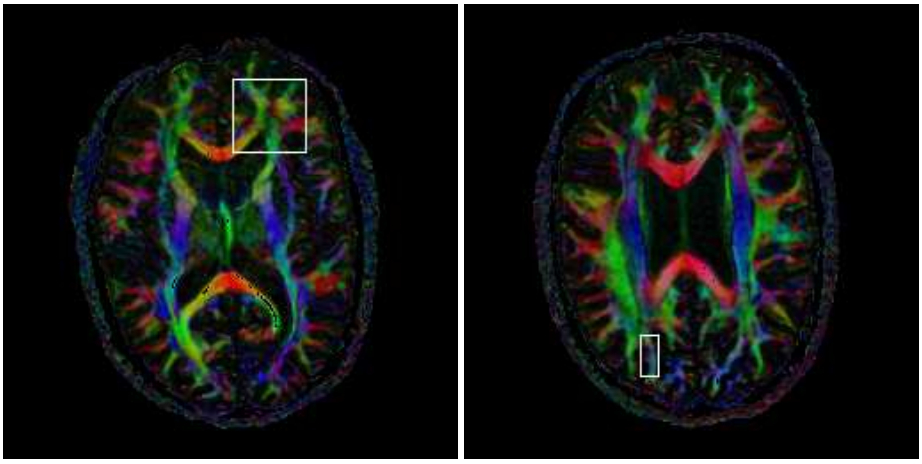

Figure 9: Color coded FA with location for data cubes of data set 1 (left) and data set 2 (right). Information shown is within slice three of the sub cubes.

Data set 3: An artificial data set created by demo(dti_art) with default settings. For this data set the tensor model is adequate.

Data directory: data3

Dimension: $64 \times 64 \times 30$

Gradient-File: access from package by

```
data("optgradients")
gradients <- cbind(matrix(0,3,1),optgrad[[16]])
```

Number of gradients: 22 (1 zero, 21 directions)

Data set 4: An artificial data set created by demo(mixtens_art) with default settings (except $n = 7$).

Data directory: data4a (without noise) and data4b (with $SNR = 50$)

Dimension: $7 \times 7 \times 7$

Gradient-File: access from package by

```
data("optgradients")
gradients <- cbind(matrix(0,3,7),optgrad[[131]])
```

Number of gradients: 143 (7 zero, 136 directions)

Data set 5: Fibertracks identified from whole brain data recorded within an diffusion weighted experiment by H.-U. Voss using a tensor mixture model of maximal order 5. The data set contains fibers extending over at least 100 voxel. Access data using `load("tracks100.rsc")`.

B Code used for the examples and illustrations

In this appendix we provide code used to generate illustrations and evaluation of examples. This code is also available in the electronic supplements in file `examples.r`.

Code for Figure 1:

```
library(dti)
data("optgradients")
gradients <- cbind(matrix(0,3,1),optgrad[[16]])
dwiobj <- readDWIdata(gradients,"data3","NIFTI")
show3d(dwiobj[26:30,26,15],bg="white",what="data")
rgl.snapshot("dwidata.png")
```

Code for Figure 2:

```
library(dti)
data("optgradients")
gradients <- cbind(matrix(0, 3, 7), optgrad[[131]])
dwiobj <- readDWIdata(gradients, "data4a", "NIFTI")
#   this is data without noise
#   and may be used to construct the true ODF
dwiobj <- sdpar(dwiobj, 200, interactive = FALSE)
mixtens3 <- dwiMixtensor(dwiobj[5, 5, 5], maxcomp = 5)
qballobj2 <- dwiQball(dwiobj[5, 5, 5], order = 2, lambda = 0)
qballobj4 <- dwiQball(dwiobj[5, 5, 5], order = 4, lambda = 0)
qballobj6 <- dwiQball(dwiobj[5, 5, 5], order = 6, lambda = 0)
qballobj8 <- dwiQball(dwiobj[5, 5, 5], order = 8, lambda = 0)
source(system.file("rcode/mousecallbacks.r", package = "dti"))
sizex <- 320
sizey <- 320
w1 <- show3d(mixtens3, subdivide = 4, FOV = 1,
             windowRect = c(1, 1, sizex, sizey))
w2 <- show3d(qballobj2, subdivide = 4, FOV = 1,
             windowRect = c(sizex+11, 1, 2*sizex+10, sizey))
w3 <- show3d(qballobj4, subdivide = 4, FOV = 1,
             windowRect = c(2*sizex+21, 1, 3*sizex+20, sizey))
w4 <- show3d(qballobj6, subdivide = 4, FOV = 1,
             windowRect = c(3*sizex+31, 1, 4*sizex+30, sizey))
w5 <- show3d(qballobj8, subdivide = 4, FOV = 1,
             windowRect = c(4*sizex+41, 1, 5*sizex+40, sizey))
mouseTrackball(dev = c(w1, w2, w3, w4, w5))
mouseZoom(2, dev = c(w1, w2, w3, w4, w5))
mouseFOV(3, dev = c(w1, w2, w3, w4, w5))
cat("w1 - true ODF
   \nw2 - Expected ODF estimate by Spherical harmonics
          approximation order 2 without regularization
   \nw3 - Expected ODF estimate by Spherical harmonics
          approximation order 4 without regularization
   \nw4 - Expected ODF estimate by Spherical harmonics
          approximation order 6 without regularization
   \nw5 - Expected ODF estimate by Spherical harmonics
          approximation order 8 without regularization")
rgl.set(w1)
```

```
rgl.snapshot("truemix3.png")
rgl.set(w2)
rgl.snapshot("ExpectedODF2.png")
rgl.set(w3)
rgl.snapshot("ExpectedODF4.png")
rgl.set(w4)
rgl.snapshot("ExpectedODF6.png")
rgl.set(w5)
rgl.snapshot("ExpectedODF8.png")
```

Code for Example 3.1.1:

```
library(dti)
data("optgradients")
gradients <- cbind(matrix(0, 3, 1), optgrad[[16]])
dwiobj <- readDWIdata(gradients, "data3", "NIFTI")
dwiobj <- sdpar(dwiobj, 100)
dtiobj <- dtiTensor(dwiobj) # Tensor estimation
dtiind <- dtiIndices(dtiobj) # Tensor characteristics
dtiobj.smooth <- dti.smooth(dwiobj, hmax = 4)
# Tensor estimation with adapt. smoothing
# Tensor characteristics
dtiind.smooth <- dtiIndices(dtiobj.smooth)
# Fiber tracking
tracks <- tracking(dtiobj, minfa = .2)
# remove redundant fibers
tracks <- reduceFibers(tracks, maxdist = .5)
tracks.smooth <- reduceFibers(tracking(dtiobj.smooth, minfa = .2),
                              maxdist = .5)
source(system.file("rcode/mousecallbacks.r", package="dti"))
sizex <- 400
sizey <- 450
w1 <- show3d(dtiind, FOV = 1,
             windowRect = c(1, 1, sizex, sizey))
w2 <- show3d(dtiind.smooth, FOV = 1,
             windowRect = c(sizex+11, 1, 2*sizex+10, sizey))
w3 <- show3d(tracks, FOV = 1,
             windowRect = c(2*sizex+21, 1, 3*sizex+20, sizey))
w4 <- show3d(tracks.smooth, FOV = 1,
             windowRect = c(3*sizex+31, 1, 4*sizex+30, sizey))
mouseTrackball(dev = c(w1, w2, w3, w4))
mouseZoom(2, dev = c(w1, w2, w3, w4))
mouseFOV(3, dev = c(w1, w2, w3, w4))
cat("w1 - Fiber orientations from tensor estimates
   \nw2 - Fiber orientations from smoothed tensor estimates
   \nw3 - Tracking results from tensor estimates
   \nw4 - Tracking results from smoothed tensor estimates
   \n   - Color codes orientation:
            red - along x; green - along y; blue - along z")
rgl.set(w1)
rgl.snapshot("ex1tens.png")
rgl.set(w2)
rgl.snapshot("ex1smtens.png")
rgl.set(w3)
```

```
rgl.snapshot("ex1tracks.png")
rgl.set(w4)
rgl.snapshot("ex1smtracks.png")
```

Code for Example 3.1.2:

```
library(dti)
gradients <- read.table("b-directions.txt")
dwiobj <- readDWIdata(gradients, "data1", "NIFTI")
dwiobj <- sdpar(dwiobj, 500, interactive = FALSE)
mixtensobj <- dwiMixtensor(dwiobj, maxcomp = 4) # approx. 6 min.
dwiqball8.25m3 <- dwiQball(dwiobj, order = 8, lambda = 2.5e-3)
dwiqball8.1m2 <- dwiQball(dwiobj, order = 8, lambda = 1e-2)
dwiqball8.4m2 <- dwiQball(dwiobj, order = 8, lambda = 4e-2)
coord <- plot(mixtensobj, slice = 3, what = "eorder",
              view = "axial", identify = TRUE)
# get coordinates of two interesting voxel
# (here c(17,10,3) and c(23,12,3))
# Visualize results for order 2 voxel
source(system.file("rcode/mousecallbacks.r", package = "dti"))
sizex <- 400
sizey <- 400
w1 <- show3d(mixtensobj[17, 10, 3],
             windowRect = c(1, 1, sizex, sizey))
w2 <- show3d(dwiqball8.25m3[17, 10, 3],
             windowRect = c(sizex+11, 1, 2*sizex+10, sizey))
w3 <- show3d(dwiqball8.1m2[17, 10, 3],
             windowRect = c(2*sizex+21, 1, 3*sizex+20, sizey))
w4 <- show3d(dwiqball8.4m2[17, 10, 3],
             windowRect = c(3*sizex+31, 1, 4*sizex+30, sizey))
mouseTrackball(dev = c(w1, w2, w3, w4))
mouseZoom(2,dev = c(w1, w2, w3, w4))
mouseFOV(3,dev = c(w1, w2, w3, w4))
rgl.set(w1)
rgl.snapshot("ex2mix2.png")
rgl.set(w2)
rgl.snapshot("ex2qball2a.png")
rgl.set(w3)
rgl.snapshot("ex2qball2b.png")
rgl.set(w4)
rgl.snapshot("ex2qball2c.png")
# Visualize results for order 3 voxel
w5 <- show3d(mixtensobj[23, 12, 3],
             windowRect = c(1, sizey+11,
                            sizex, 2*sizey+10))
w6 <- show3d(dwiqball8.25m3[23, 12, 3],
             windowRect = c(sizex+11, sizey+11,
                            2*sizex+10, 2*sizey+10))
w7 <- show3d(dwiqball8.1m2[23, 12, 3],
             windowRect = c(2*sizex+21, sizey+11,
                            3*sizex+20, 2*sizey+10))
w8 <- show3d(dwiqball8.4m2[23, 12, 3],
             windowRect = c(3*sizex+31, sizey+11,
                            4*sizex+30, 2*sizey+10))
```

```
mouseTrackball(dev = c(w5, w6, w7, w8))
mouseZoom(2, dev = c(w5, w6, w7, w8))
mouseFOV(3, dev = c(w5, w6, w7, w8))
rgl.set(w5)
rgl.snapshot("ex2mix3.png")
rgl.set(w6)
rgl.snapshot("ex2qball3a.png")
rgl.set(w7)
rgl.snapshot("ex2qball3b.png")
rgl.set(w8)
rgl.snapshot("ex2qball3c.png")
```

Code for Example 3.1.3:

```
library(dti)
gradients <- read.table("b-directions.txt")
dwiobj <- readDWIdata(gradients, "data2", "NIFTI")
dwiobj <- sdpar(dwiobj, 500, interactive = FALSE)
tensobj <- dtiTensor(dwiobj)
summary(tensobj)# summary information
indobj <- dtiIndices(tensobj)
summary(indobj)# summary information
img0 <- plot(indobj, slice = 2, what = "fa", view = "axial")
mixtensobj <- dwiMixtensor(dwiobj, maxcomp = 5) # approx. 90s
summary(mixtensobj) # summary information
img1 <- plot(mixtensobj, slice = 2, what = "fa", view = "axial")
img2 <- plot(mixtensobj, slice = 2, what = "order", view = "axial")
img3 <- plot(mixtensobj, slice = 2, what = "eorder", view = "axial")
img4 <- plot(mixtensobj, slice = 2, what = "ev", view = "axial")
X11(width = 1000, height = 500)
par(mfrow=c(1,5),mar=c(1,1,3,.2),mgp=c(2,1,0))
show.image(img0, main = "Tensor FA")
show.image(img1, main = "Mixture FA")
show.image(img2, main = "Mixture order")
show.image(img3, main = "Effective order")
show.image(img4, main = "Maximum Eigenvalue")
write.image(img0, file = "ex3tensfa.png")
write.image(img1, file = "ex3mixfa.png")
write.image(img2, file = "ex3mixord.png")
write.image(img3, file = "ex3mixeo.png")
write.image(img4, file = "ex3mixev.png")
w1 <- show3d(mixtensobj, maxangle = 45, fibers = TRUE, mineo = 1.8,
             FOV = 1, windowRect = c(1, 1, 1000, 600), lwd = 3)
rgl.snapshot("eo1.8regionmix5.png")
```

Code for Example 3.1.4:

```
library(dti)
load("tracks100.rsc")
summary(tracks100)
show3d(tracks100)
```